Hemipterous/D-MKK7 mediate the activation of D-JNK by cadmium and arsenite in Schneider cells. *BMC Cell Biol.* **7**, 7.

Sreedharan J., Blair I. P., Tripathi V. B. *et al.* (2008) TDP-43 mutations in familial and sporadic amyotrophic lateral sclerosis. *Science* **319**, 1668–1672.

Stoecklin G., Stubbs T., Kedersha N., Wax S., Rigby W. F., Blackwell T. K. and Anderson P. (2004) MK2-induced tristetraprolin:14–3-3 complexes prevent stress granule association and ARE-mRNA decay. *EMBO J.* **23**, 1313–1324.

Udan M. and Baloh R. H. (2011) Implications of the prion-related Q/N domains in TDP-43 and FUS. *Prion* **5**, 1–5.

Vance C., Rogelj B., Hortobagyi T. *et al.* (2009) Mutations in FUS, an RNA processing protein, cause familial amyotrophic lateral sclerosis type 6. *Science* **323**, 1208–1211.

Xu Z. S. (2012) Does a loss of TDP-43 function cause neurodegeneration? *Mol. Neurodegener.* **7**, 27.

Zhang Y. J., Xu Y. F., Dickey C. A., Buratti E., Baralle F., Bailey R., Pickering-Brown S., Dickson D. and Petrucelli L. (2007) Progranulin mediates caspase-dependent cleavage of TAR DNA binding protein-43. *J. Neurosci.* **27**, 10530–10534.

TDP-43 associates with stalled ribosomes and contributes to cell survival during cellular stress.

Shinji Higashi, Tomohiro Kabuta, Yoshitaka Nagai, Yukihiro Tsuchiya, Haruhiko Akiyama, Keiji Wada

Supporting Information

Supplemental Methods

Cell culture and transfection

HeLa or SH-SY5Y cells were maintained in Dulbecco's modified Eagle's medium (Invitrogen, Carlsbad, CA, USA) supplemented with 10% fetal bovine serum (FBS). Transient transfection of cultured cells with each vector was performed using the Lipofectamine LTX Reagent (Invitrogen) according to the manufacturer's instructions. Plasmids and reagents applied in this study are described in the supporting information.

Plasmids

pFLAG-CMV hTDP-43 plasmids for expressing wild-type (WT) TDP-43 or amino acid residues 2–272 ($TDP_{2\text{-}272}$) or 101–414 ($TDP_{101\text{-}414}$) of TDP-43 with a FLAG tag at the N-terminus, as shown in Fig. 6E, were prepared as previously described (Higashi et al. 2010b). To make pCI-neo hTDP-43 plasmids for expressing amino acid residues 202–414 ($TDP_{202\text{-}414}$) of TDP-43 with a FLAG tag at the C-terminus, truncated TDP-43 fragments were amplified by PCR using the using the following primers: forward, 5'-AAAACTCGAGCCGCCACCATGATCGAGGATGAGCTGCGGG-3' and reverse, 5'-AAAAGCGGCCGCTTACTTGTCATCGTCGTCCTTGTAGTCCATTCCCCAGCCAGAAGACTTAG-3'. pCI-neo hTDP-43 plasmids for expressing WT TDP-43 with FLAG at the N-terminus (Fig. 7B) were amplified by PCR using the using the following primers: forward, 5'-AAAACTCGAGCCGCCACCATGGACTACAAGGACGACGATGACAAGTCTGAATATATTCGGGTAACCGAAG-3' and reverse, 5'-AAAAGCGGCCGCCTACATTCCCCAGCCAGAAGAC-3'. The PCR products were digested with XhoI and NotI and cloned into XhoI/NotI-digested pCI-neo expression vector (Promega, Madison, WI, USA). pCI-neo hTDP-43 for expressing mutant Ala TDP-43, in which serines 403/404/409/410 were replaced with alanines, with FLAG at the N-terminus (Fig. 7B), was generated using the Quik-Change Mutagenesis kit (Stratagene, La Jolla, CA) according to the manufacturer's instructions. All resulting constructs were confirmed by sequencing.

Reagents

Sodium arsenite (ARS) and the general caspase inhibitor Q-VD-OPh, were purchased from Sigma-Aldrich (St. Louis, MO) and R&D Systems, Inc. (Minneapolis, MN), respectively. SP600123, SB203580 and PD98059 were purchased from Calbiochem Corp. (La Jolla, CA).

Antibodies

The following primary antibodies were used: rabbit polyclonal anti-TDP-43 raised to the C terminus of TDP-43 (Higashi *et al.* 2010b); rabbit polyclonal phosphorylated TDP-43 (Ser403/404 or Ser409/410) and mouse monoclonal anti-phosphorylated TDP-43 (Ser409/410) were raised as previously described (Hasegawa *et al.* 2008, Inukai *et al.* 2008); mouse monoclonal anti-FUS/TLS (4H11, Santa Cruz Biotechnology, Santa Cruz, CA); goat polyclonal anti-TIA-1 (Santa Cruz Biotechnology); mouse monoclonal anti-HuR (Santa Cruz Biotechnology); rabbit polyclonal anti-L7a (Santa Cruz Biotechnology); goat polyclonal anti-eIF3η (Santa Cruz Biotechnology); rabbit monoclonal anti-S6 (5G10, Cell Signalling Technology, Tokyo, Japan); rabbit polyclonal anti-phosphorylated p44/42 MAPK (ERK1/2) (Thr202/Tyr204) (Cell Signalling Technology); rabbit monoclonal anti-phosphorylated p38 MAPK (Thr180/Tyr182) (12F8, Cell Signalling Technology); rabbit polyclonal anti-phosphorylated SAPK/JNK (Thr183/Tyr185) (Cell Signalling Technology); rabbit polyclonal anti-cleaved caspase-3 (Asp175) (Cell Signalling Technology); guinea pig polyclonal anti-p62 (Progen Biotechnik. Heidelberg, Germany), mouse monoclonal anti-Dcp1a (3G4, Abnova Corp., Taipei, Taiwan); rabbit polyclonal anti-G3BP1 (Sigma-Aldrich, St. Louis, MO) and mouse monoclonal anti-β-actin (AC-15, Sigma-Aldrich).

Western blotting

HeLa cells were harvested in cold Triton X-100 lysis buffer (50mM Tris-HCl pH 7.5, 150mM NaCl, 5mM EDTA, 1% Triton X-100 and Complete protease inhibitors [Roche, Tokyo, Japan]). Lysates were rotated at 4°C for 1 h, and Triton X-100-soluble supernatant fractions were obtained by centrifugation at 20,000 × g for 15 min at 4°C. Triton X-100-insoluble fractions were obtained by sonicating the pellets with SDS sample buffer (10mM Tris-HCl, pH 7.8, 3% SDS, 5% glycerol, 0.02% bromophenol blue and 2% 2-mercaptoethanol).

For sequential extraction, Triton X-100-insoluble pellet were washed once in Triton X-100 lysis buffer and then solubilized by pipetting and vortex in Sarkosyl (SARK) lysis

buffer (50mM Tris-HCl pH 7.5, 15 mM NaCl, 5mM EDTA, 1% (w/v) N-lauroyl-sarcosine and Complete protease inhibitors) for 30 min at RT. After additional centrifuge at 100,000× g for 15 min, supernatant fractions (SARK fraction) were collected. Remaining pellets were extracted by sonication in urea lysis buffer (7M urea, 2M tiourea, 4% 3-[(3-cholamidopro-pyl)dimethylammonio]-1-propanesulfonate (CHAPS) and 30mM Tris-HCl pH 8.5) and then saved as urea fraction.
Protein samples were separated by SDS–PAGE and transferred from gels to PVDF membranes (Bio-Rad, Tokyo, Japan) and analyzed by western blotting as previously described (Higashi *et al.* 2010a).

Immunocytochemistry

HeLa cells were grown in two-chamber culture slides to about 50% confluence. After incubation with each reagent, cells were rinsed with Tris-buffered saline (TBS), fixed with 4% paraformaldehyde for 20 min, permeabilized with 0.2% Triton X-100/0.02% bovine serum albumin (BSA) in TBS for 10 min at 4°C, and then blocked for 30 min at RT with 3% BSA/0.02% Triton X-100 in TBS (blocking solution). Cells were incubated overnight at 4°C with primary antibodies at the appropriate dilution in blocking solution. After washing with TBS, sections were incubated for 2 h with Cy^{TM}2-, Cy^{TM}3-, or Cy^{TM}5-conjugated secondary antibodies (Jackson ImmunoResearch Lab, Inc., Baltimore Pike, PO) at 1:200–400 dilutions in blocking buffer. After incubating with 4',6-diamidino-2-phenylindole for 2 min, the coverslips were washed with TBS and mounted in mounting medium.

siRNA experiments

Short interfering RNA (siRNA) experiments were performed as previously described (Higashi et al. 2010a). HeLa cells were seeded in complete medium without antibiotics at a density of 1×10^6 cells per well in 10-cm dishes or at 1×10^5 cells per well in 6 well plates, and SH–SY5Y cells were seeded at 2.5×10^5 cells per well in 6-well plates or at 2.5×10^5 cells per chamber in two-chamber culture slides. Both types of cells were transfected using Lipofectamine RNAiMAX (Invitrogen) according to the manufacturer's instructions. To transfect HeLa cells, 60 pmol (for 10-cm dishes) or 15 pmol (for 6-well plates) of siRNA duplex of TDP-43 3' untranslated region (sense, 5'-CAUUUUUAUCCGCUACUCUUU -3'; anti-sense, 5'-AGAGUAGCGGAUAAAAAUGGG -3'), or enhanced green fluorescent protein (EGFP) (sense, 5'-GCCACAACGUCUAUAUCAUGG-3'; anti-sense, 5'-AUGAUAUAGACGUUGUGGCUG-3') was applied to each well. For SH-SY5Y cells, 75 pmol (for 6-well plates) or 15 pmol (for two-chamber culture slides) of siRNA duplex were applied to each well. EGFP siRNA was used as a control. siRNAs were

purchased from RNAi Co., Ltd. (Tokyo, Japan). Sequences targeted by siRNA were selected using siDirect (RNAi Co., Ltd). Three or 4 days after transfection, the cells were treated with ARS, and then harvested for western blotting, polysome profile analysis or LDH cytotoxicity assay.

Quantitative assessment of cell death

Control or TDP-43-silenced cells were prepared in 6-well plates as described above. Both types of cells were treated with ARS (0.5 mM or 0.25 mM ARS were applied to HeLa or SH-SY5Y cells, respectively) in complete medium without antibiotics for 2 h and then incubated in ARS-free 1% FBS medium without antibiotics for 8 h. Cell death was assessed by a LDH release assay using the LDH Cytotoxicity Detection kit (Takara, Tokyo Japan) according to the manufacturer's instructions. In addition to luminescence value showing LDH release from control siRNA- or TDP-43 siRNA-transfected cells treated with ARS, the percentage of cytotoxicity was also calculated according to the instructions (Fig. 5c,d). In brief, to calculate the percentage of cytotoxicity, we prepared three controls, including a background control, a low control and a high control. The low control is LDH activity released from ARS-untreated control siRNA- or TDP-43 siRNA-transfected cells to measure spontaneous LDH release. The high control is LDH release induced by the addition of Triton X-100 to measure the maximum releasable LDH activity. We determined the percent cytotoxicity as follows:

$$\text{Percent cytotoxicity} = \frac{\text{experimental value - low control}}{\text{high control - low control}} \times 100$$

Supplemental Figures

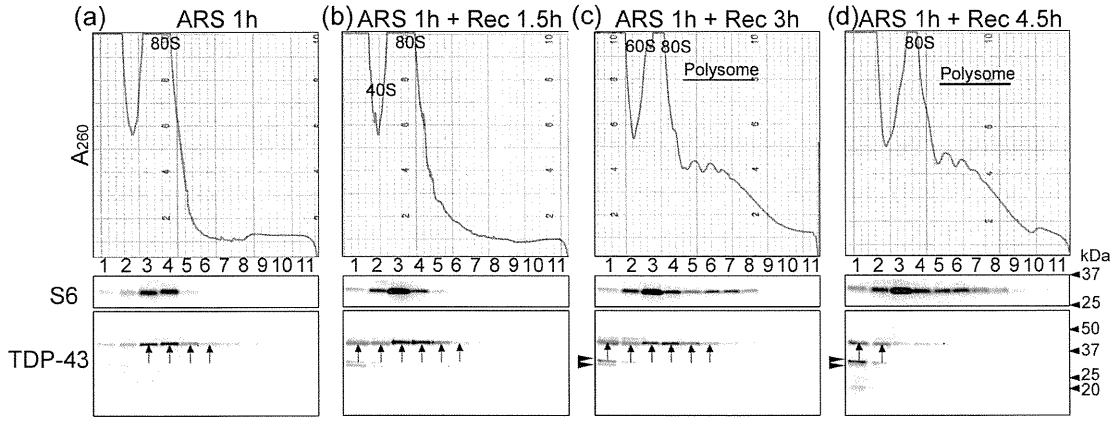

Fig. S1 (a–d) Cell extracts obtained from HeLa cells treated with 0.5 mM ARS for 1 hour (h) (a), or treated with 0.5 mM ARS for 1 h and then allowed to recover in ARS-free media (denoted as Rec) for the indicated times (b-d) were subjected to polysome profile analysis, and then immunoblot analysis with anti-S6 (small ribosomal subunits) or anti-TDP-43 (recognizing the carboxyl (C)-terminal region) antibodies. Arrows or arrowheads indicate the distribution of full-length or C-terminal (approximately 31 kDa and 33 kDa) TDP-43 in the gradient, respectively.

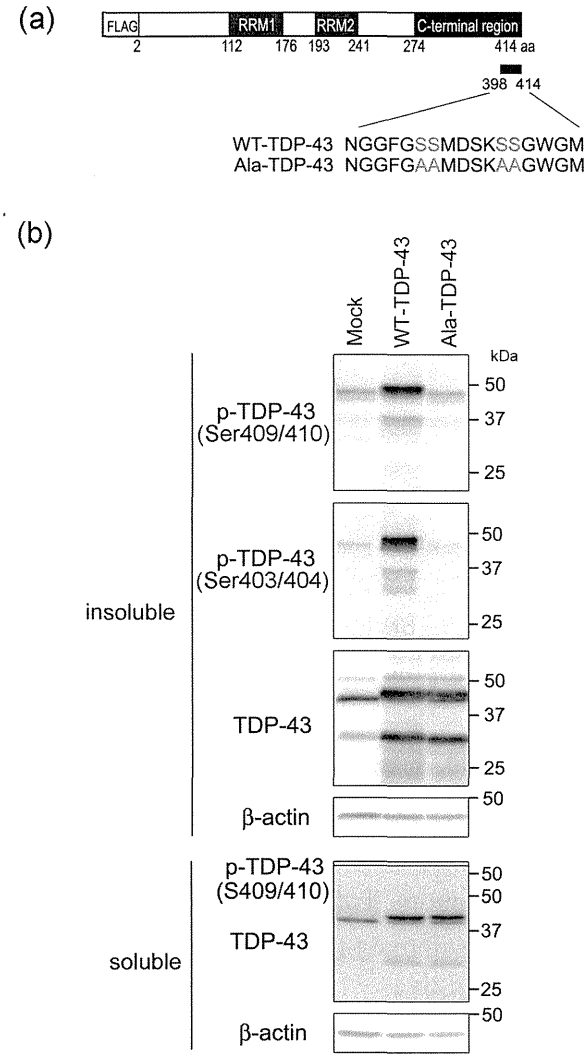

Fig. S2 (a) The domain architectures of wild-type (WT) TDP-43 or TDP-43 bearing mutation of serines (Ser403/404/409/410) to alanines (Ala) are shown schematically. **(b)** HeLa cells were transiently transfected with empty (Mock), WT or Ala TDP-43 and then treated with 0.5 mM ARS for 2 h followed by recovery in ARS-free media for 4.5 h, extracted with 1% Triton X-100 lysis buffer, and then subjected to immunoblotting with anti-p-TDP-43 (Ser409/410 or Ser403/404), anti-TDP-43 or anti-β-actin antibody.

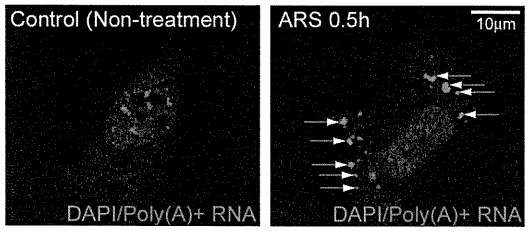

Fig. S3 SH-SY5Y neuronal cells were untreated (Control) or treated with 0.25 mM ARS for 0.5 h, and then analyzed by fluorescence *in situ* hybridization, as indicated. Arrows indicate stress granules (SGs). DAPI, 4', 6-diamidino-2-phenylindole.

References

Hasegawa, M., Arai, T., Nonaka, T. et al. (2008) Phosphorylated TDP-43 in frontotemporal lobar degeneration and amyotrophic lateral sclerosis. *Ann Neurol,* 64, 60-70.

Higashi, S., Iseki, E., Minegishi, M., Togo, T., Kabuta, T. and Wada, K. (2010a) GIGYF2 is present in endosomal compartments in the mammalian brains and enhances IGF-1-induced ERK1/2 activation. *J Neurochem,* 115, 423-437.

Higashi, S., Tsuchiya, Y., Araki, T., Wada, K. and Kabuta, T. (2010b) TDP-43 physically interacts with amyotrophic lateral sclerosis-linked mutant CuZn superoxide dismutase. *Neurochem Int,* 57, 906-913.

Inukai, Y., Nonaka, T., Arai, T. et al. (2008) Abnormal phosphorylation of Ser409/410 of TDP-43 in FTLD-U and ALS. *FEBS Lett,* 582, 2899-2904.

OPEN ACCESS Freely available online

PLOS ONE

Hsp40 Gene Therapy Exerts Therapeutic Effects on Polyglutamine Disease Mice via a Non-Cell Autonomous Mechanism

H. Akiko Popiel[1], Toshihide Takeuchi[1], Hiromi Fujita[1], Kazuhiro Yamamoto[2], Chiyomi Ito[3], Hiroshi Yamane[1], Shin-ichi Muramatsu[4], Tatsushi Toda[3], Keiji Wada[1], Yoshitaka Nagai[1,5]*

1 Department of Degenerative Neurological Diseases, National Institute of Neuroscience, National Center of Neurology and Psychiatry, Kodaira, Tokyo, Japan, **2** Division of Laboratory Animals Resources, National Institute of Neuroscience, National Center of Neurology and Psychiatry, Kodaira, Tokyo, Japan, **3** Division of Neurology/Molecular Brain Science, Kobe University Graduate School of Medicine, Kobe, Hyogo, Japan, **4** Division of Neurology, Department of Medicine, Jichi Medical University, Shimotsuke, Tochigi, Japan, **5** Core Research for Evolutional Science and Technology (CREST), Japan Science and Technology Agency, Kawaguchi, Saitama, Japan

Abstract

The polyglutamine (polyQ) diseases such as Huntington's disease (HD), are neurodegenerative diseases caused by proteins with an expanded polyQ stretch, which misfold and aggregate, and eventually accumulate as inclusion bodies within neurons. Molecules that inhibit polyQ protein misfolding/aggregation, such as Polyglutamine Binding Peptide 1 (QBP1) and molecular chaperones, have been shown to exert therapeutic effects *in vivo* by crossing of transgenic animals. Towards developing a therapy using these aggregation inhibitors, we here investigated the effect of viral vector-mediated gene therapy using QBP1 and molecular chaperones on polyQ disease model mice. We found that injection of adeno-associated virus type 5 (AAV5) expressing QBP1 or Hsp40 into the striatum both dramatically suppresses inclusion body formation in the HD mouse R6/2. AAV5-Hsp40 injection also ameliorated the motor impairment and extended the lifespan of R6/2 mice. Unexpectedly, we found even in virus non-infected cells that AAV5-Hsp40 appreciably suppresses inclusion body formation, suggesting a non-cell autonomous therapeutic effect. We further show that Hsp40 inhibits secretion of the polyQ protein from cultured cells, implying that it inhibits the recently suggested cell-cell transmission of the polyQ protein. Our results demonstrate for the first time the therapeutic effect of Hsp40 gene therapy on the neurological phenotypes of polyQ disease mice.

Citation: Popiel HA, Takeuchi T, Fujita H, Yamamoto K, Ito C, et al. (2012) Hsp40 Gene Therapy Exerts Therapeutic Effects on Polyglutamine Disease Mice via a Non-Cell Autonomous Mechanism. PLoS ONE 7(11): e51069. doi:10.1371/journal.pone.0051069

Editor: Hitoshi Okazawa, Tokyo Medical and Dental University, Japan

Received July 18, 2012; **Accepted** October 29, 2012; **Published** November 30, 2012

Funding: This work was supported in part by Grants-in-Aid for Scientific Research on Priority Areas (Research on Pathomechanisms of Brain Disorders and Protein Community to Y.N.), and on Innovative Areas (Synapse and Neurocircuit Pathology to Y.N. and S.M.) and by a Comprehensive Brain Science Network Award for Young Scientists to H.A.P., from the Ministry of Education, Culture, Sports, Science, and Technology, Japan; by Grants-in-Aid for Scientific Research (B) to Y.N., for Young Scientists (B) to H.A.P., from the Japan Society for the Promotion of Science, Japan; by a Grant-in-Aid for the Research Committee for Ataxic Diseases to Y.N. and a Grant-in-Aid for the Research Committee of CNS Degenerative Diseases to S.M. from the Ministry of Health, Labor and Welfare, Japan. The funders had no role in study design, data collection and analysis, decision to publish, or preparation of the manuscript.

Competing Interests: Co-author Yoshitaka Nagai is a PLOS ONE Editorial Board member. This does not alter the authors' adherence to all the PLOS ONE policies on sharing data and materials.

* E-mail: nagai@ncnp.go.jp

Introduction

The polyglutamine (polyQ) diseases are a group of inherited neurodegenerative disorders that are all caused by a common genetic mutation, namely an expansion (>40) of a polyQ-encoding CAG repeat in each unrelated disease-causing gene [1,2]. Nine polyQ diseases have been identified to date, including Huntington's disease (HD), spinocerebellar ataxia (SCA) types 1, 2, 3, 6, 7, 17, dentatorubral pallidoluysian atrophy (DRPLA), and spinobulbar muscular atrophy (SBMA). In these disorders, progressive degeneration of neurons in brain areas specific for each disorder occurs, causing various neurological and psychiatric symptoms corresponding to each affected brain area [1,2].

In the common molecular pathogenesis of the polyQ diseases, proteins with an expanded polyQ stretch become misfolded and form aggregates, and subsequently accumulate as inclusion bodies within neurons, eventually resulting in neurodegeneration [3–7]. Moreover, recent studies suggest that prion-like transmission of aggregation-prone proteins between cells is involved in neuropathological spreading during disease progression in not only the polyQ diseases but also various other neurodegenerative diseases [8–11]. Although various therapeutic strategies against downstream targets of the pathogenic cascade have been investigated, misfolding and aggregation of the polyQ protein are ideal therapeutic targets since they are the most initial pathogenic events, and therefore their inhibition is expected to result in the suppression of a broad range of downstream pathogenic events [3,5,12,13].

In our attempt to establish a therapy for the polyQ diseases, we hypothesized that molecules that specifically bind to the expanded polyQ stretch would suppress misfolding and aggregation of the expanded polyQ protein. Accordingly, by phage display screening of combinatorial peptide libraries, we identified PolyQ Binding Peptide 1 (QBP1), and proved that QBP1 indeed inhibits polyQ protein misfolding/aggregation *in vitro* [14–16]. Furthermore, we

demonstrated that expression of QBP1 suppresses neurodegeneration *in vivo* in polyQ disease model animals [16,17]. Another approach for targeting misfolding and aggregation of the expanded polyQ protein is to utilize molecular chaperones, which are a group of biomolecules that assist the proper folding of proteins and prevent protein misfolding/aggregation [18–20]. Indeed, overexpression of molecular chaperones such as Hsp40 and Hsp70 has been shown to suppress polyQ protein aggregation and polyQ-induced neurodegeneration in various animal models of the polyQ diseases, such as flies [21–24], worms [25] and mice [26–30]. However, most studies showing the therapeutic efficacy of these aggregation inhibitors have been performed by crossing transgenic animals so far. To develop a therapy using aggregation inhibitors such as QBP1 and molecular chaperones, transgenes need to be delivered in affected individuals by administration, rather than be expressed in the next generation by crossing transgenic animals.

In this study, we employed a viral vector to deliver these transgenes into the brain and investigated their therapeutic effects on polyQ disease model mice. Among various viral vectors, we chose to use adeno-associated virus vector (AAV) because of its widespread infection throughout the brain, its long-term expression of transgenes, and its safety [31,32]. We successfully demonstrate the therapeutic effects of AAV5-QBP1 and AAV5-Hsp40 injections on a mouse model of HD. Most interestingly, we found that AAV5-Hsp40 exerts a non-cell autonomous therapeutic effect, possibly via inhibition of the recently-suggested cell-cell transmission of the polyQ protein, indicating a novel therapeutic mode of action of Hsp40.

Results

AAV5-QBP1 and AAV5-Hsp40 Inhibit Inclusion Body Formation in polyQ Disease Mouse Neurons

We employed the R6/2 HD mouse model [33] to investigate the therapeutic effect of AAV-mediated expression of QBP1 and molecular chaperones. We first tested the effect on accumulation of the pathogenic polyQ protein into inclusion bodies in the neurons of R6/2 mice by AAV5 injections. Injections were performed on mice at postnatal day 7 (P7) using an infusion pump (see Materials and Methods), which has been shown to lead to widespread delivery of the injected molecules in the brain [34], and indeed resulted in widespread expression of the transgene throughout the injected brain hemisphere with ~30% infection efficiencies (Fig. S1). R6/2 mice were injected with AAV5-GFP on one side of the striatum and AAV5-QBP1 on the other side, and htt inclusion body formation was compared between the two sides of both the striatum and the cortex. Inclusion bodies were already formed in 36.0% of AAV5-GFP infected neurons in the striatum at 4 weeks of age, which increased to 68.5% at 8 weeks and 73.8% at 14 weeks, and an age dependent increase in inclusion bodies was also observed in the cortex (Fig. S2). In contrast, AAV5-QBP1 infected neurons had significantly less inclusion bodies at most time points (Fig. S2), and the rates of neurons with inclusion bodies at 8 weeks, for example, were 68.5% for GFP vs 33.7% for QBP1 ($p<0.001$) in the striatum, and 49.3% for GFP vs 27.4% for QBP1 ($p<0.001$) in the cortex (Figs. 1A,B). These results demonstrate a significant inhibitory effect of AAV5-QBP1 on inclusion body formation.

We also tested the effect of AAV5-mediated expression of a molecular chaperone on inclusion body formation. Among the various molecular chaperones, we chose to use a member of the Hsp40 family, namely DNAJB1 (referred to as Hsp40 in this study), since members of the DNAJB subfamily have been

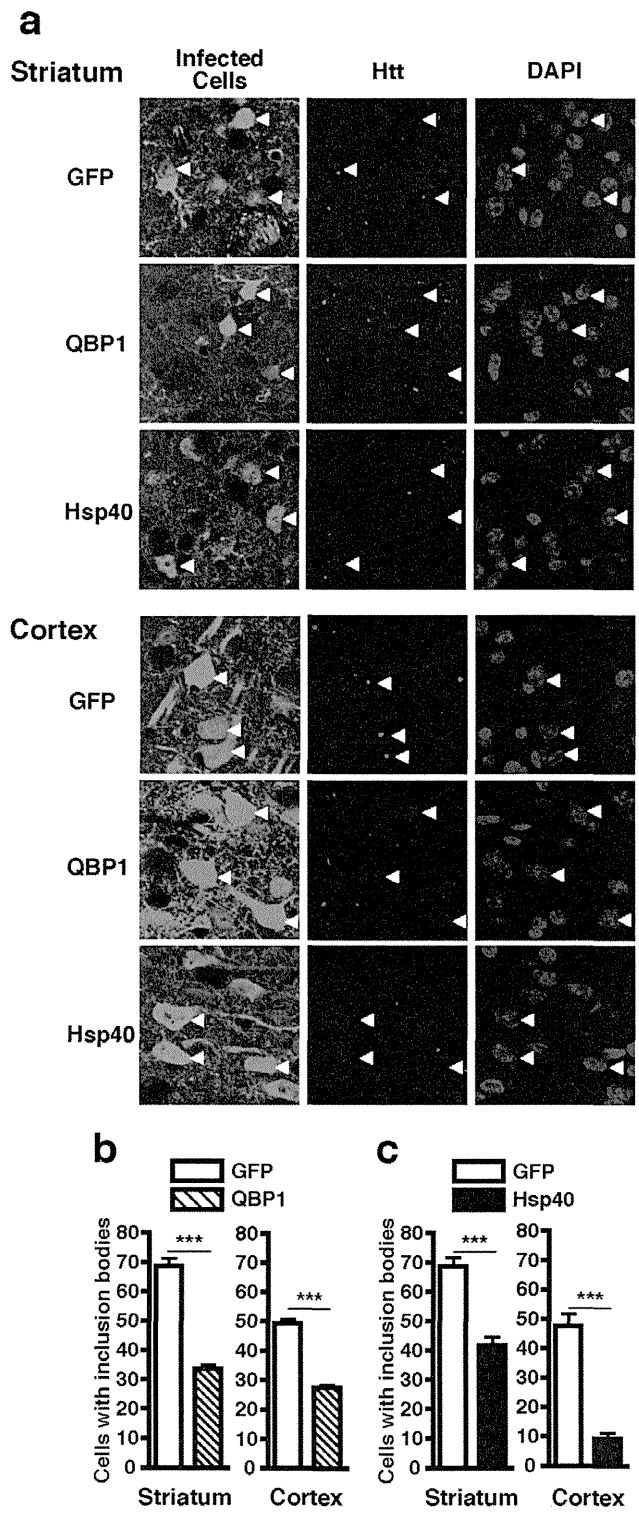

Figure 1. AAV5-QBP1 and AAV5-Hsp40 inhibit polyQ inclusion body formation in virus infected neurons of polyQ disease mice. R6/2 mice at P7 were injected with AAV5-GFP on one side of the striatum and either AAV5-QBP1 or AAV5-Hsp40 on the other side, and htt inclusion body formation in virus infected neurons was assessed at 8 weeks of age by immunohistochemistry of brain sections. (A) Representative photographs of striatal (top panels) and cortical (bottom panels) sections of R6/2 mice, injected with the indicated viruses. Green; virus infected cells, red; htt, and blue; nuclei visualized by DAPI staining. In each panel, representative virus infected cells are indicated by white

arrowheads. (B) Inclusion body formation in AAV5-QBP1 infected neurons in the striatum (left) and cortex (right). (C) Inclusion body formation in AAV5-Hsp40 infected neurons in the striatum (left) and cortex (right). In (B) and (C), data are shown as means ± SEM of ≥6 fields of view, in which over 180 cells were counted (*$p<0.05$, ***$p<0.001$). Representative results of two mice analyzed are shown.
doi:10.1371/journal.pone.0051069.g001

reported to be the most potent suppressors of expanded polyQ protein aggregation and toxicity [35]. The effect of AAV5-Hsp40 on polyQ inclusion body formation in R6/2 mice was investigated at 8 weeks, an age at which AAV5-QBP1 showed a clear inhibitory effect. AAV5-Hsp40 also exerted a robust effect on inclusion body formation, and the rates of virus infected neurons with inclusion bodies were 68.6% for GFP vs 41.7% for Hsp40 ($p<0.001$) in the striatum, and 47.5% for GFP vs 9.2% for Hsp40 ($p<0.001$) in the cortex (Figs. 1A,C). This difference in the effectiveness of Hsp40 between the two brain areas may be due to differences in the expression levels of its partner Hsp70. Although whether polyQ inclusion bodies themselves are cytotoxic or cytoprotective has been controversial [36], we assume that suppression of inclusion body formation by QBP1 and Hsp40 can be regarded as a therapeutic effect, since they act by preventing the initial toxic misfolding of the polyQ protein and promoting its refolding, respectively [15,16,19,20]. Therefore, these results collectively demonstrate that QBP1 and Hsp40 exert therapeutic effects in polyQ disease mouse neurons, via their widespread and long-term expression using AAV5.

AAV5-Hsp40 Improves Neurological Phenotypes of polyQ Disease Mice

Since our above results demonstrated that AAV5-QBP1 and AAV5-Hsp40 inhibit accumulation of the pathogenic polyQ protein into inclusions, we next tested whether this could also lead to amelioration of the neurological phenotypes of R6/2 mice. For this purpose we injected AAV5-GFP, AAV5-QBP1, or AAV5-Hsp40 into both sides of the striatum of P7 R6/2 mice, and analyzed their effects on various neurological phenotypes of these mice.

To evaluate motor impairments of R6/2 mice, we first tested their forced locomotor activity using the rotarod. Although the reduction in rotarod performance of R6/2 mice compared with wild-type (WT) mice becomes evident by 7 weeks of age, the performance of AAV5-QBP1 injected and AAV5-Hsp40 injected R6/2 mice did not significantly differ from AAV5-GFP injected mice (Fig. 2A). We further tested the effect of these viruses on spontaneous locomotor activity. R6/2 mice demonstrated significantly less open-field activity and rearing compared with WT mice as early as 5 weeks of age, which further decreased by 8 weeks. Although we could not detect a significant improvement in AAV5-QBP1 injected mice, AAV5-Hsp40 injected R6/2 mice exhibited significantly higher open-field activity and rearing compared with AAV5-GFP injected mice at 8 weeks of age (Activity: GFP 134.8±10.2 vs Hsp40 196.4±8.4 counts/min, $p<0.001$; Rearing: GFP 2.0±0.44 vs<Hsp40 6.3±0.67 counts/min, $p<0.001$) (Figs. 2B,C). These results demonstrate the therapeutic effect of AAV5-Hsp40 on the decreased spontaneous locomotor activity of R6/2 mice.

We also tested the effect of each virus on the grip strength abnormality of R6/2 mice. Grip strength of R6/2 mice was significantly weaker than that of WT mice at 9 weeks of age, and further weakened by 12 weeks of age. AAV5-QBP1 injection did not have a significant effect on grip strength at either age. In contrast, AAV5-Hsp40 injected R6/2 mice exhibited significantly

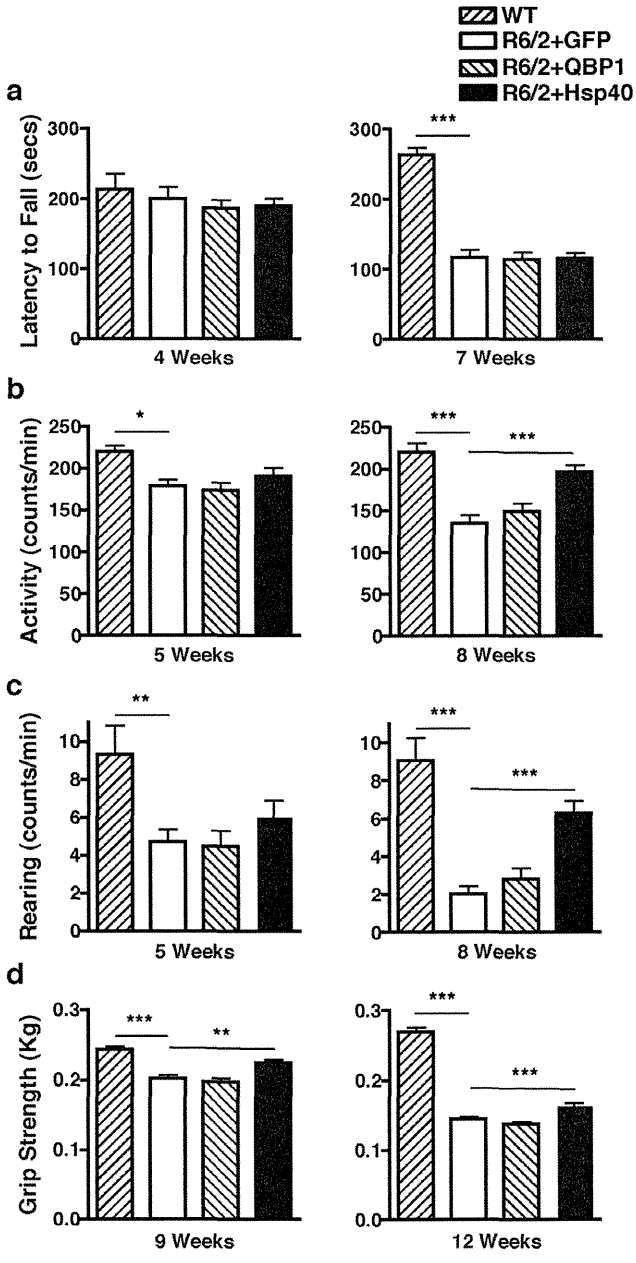

Figure 2. AAV5-Hsp40 improves spontaneous locomotor activity and grip strength abnormalities of polyQ disease mice. R6/2 mice at P7 were injected in both sides of the striatum with AAV5-GFP, AAV5-QBP1, or AAV5-Hsp40, and the following phenotypes were analyzed. (A) Rotarod performance measured at 4 (left) and 7 weeks (right) of age. (B, C) Open-field activity (B) and rearing (C) measured at 5 (left) and 8 weeks (right) of age. (D) Grip strength measured at 9 (left) and 12 weeks (right) of age. Values represent mean ± SEM, n≥9 mice (*$p<0.05$, **$p<0.01$, ***$p<0.001$).
doi:10.1371/journal.pone.0051069.g002

greater grip strengths than AAV5-GFP injected mice both at 9 weeks (GFP 0.202±0.005 vs Hsp40 0.225±0.005 Kg, $p<0.01$) and 12 weeks of age (GFP 0.145±0.003 vs Hsp40 0.165±0.003 Kg, $p<0.001$), demonstrating the therapeutic effect of AAV5-Hsp40 (Fig. 2D).

We also evaluated the body weight loss of AAV5-injected R6/2 mice. AAV5-GFP injected R6/2 mice demonstrated significantly lower body weights than WT mice after 9 weeks of age. The

weights of AAV5-QBP1 injected R6/2 mice were almost indistinguishable from AAV5-GFP injected mice at each time point. In contrast, the weights of AAV5-Hsp40 injected R6/2 mice showed a significant improvement compared to AAV5-GFP injected mice between 9 and 13 weeks of age (Fig. 3A). These results demonstrate the therapeutic effect of AAV5-Hsp40 also against the weight loss of R6/2 mice.

We then assessed the effect of AAV5 injections on the lifespan of R6/2 mice. The survival of AAV5-QBP1 injected R6/2 mice (median lifespan 100 days) was not significantly different from AAV5-GFP injected mice (median lifespan 95 days). In contrast, AAV5-Hsp40 injection resulted in a rightward shift of the survival curve to a median lifespan of 112 days, demonstrating the therapeutic effect of AAV5-Hsp40 on the decreased survival of R6/2 mice (Fig. 3B). Taken together, these results clearly demonstrate that AAV5-Hsp40 significantly improves many neurological phenotypes of R6/2 mice.

AAV5-Hsp40 Inhibits Inclusion Body Formation also in Virus Non-infected Neurons of polyQ Disease Mice

When analyzing the effect of the viruses on inclusion body formation in R6/2 mice (Fig. 1), we suspected that on the AAV5-Hsp40 injected side, not only virus infected neurons, but even virus non-infected neurons appeared to have fewer inclusion bodies than those on the AAV5-GFP injected side. To clarify our suspicion, we focused on the virus non-infected neurons that are not stained with Hsp40 or GFP antibodies (see Materials and Methods and Fig. S3), and reanalyzed inclusion body formation in the virus non-infected neurons. On the AAV5-QBP1 injected side, virus non-infected neurons showed a similar rate of inclusion body formation as non-infected neurons on the AAV5-GFP injected side, in both the striatum and cortex, as expected (Fig. 4). Surprisingly, we found that on the AAV5-Hsp40 injected side, virus non-infected neurons had strikingly fewer inclusion bodies compared with non-infected neurons on the AAV5-GFP injected side in both the striatum (GFP side 69.0% vs Hsp40 side 49.8%, $p<0.01$) and cortex (GFP side 59.1% vs Hsp40 side 39.6%,

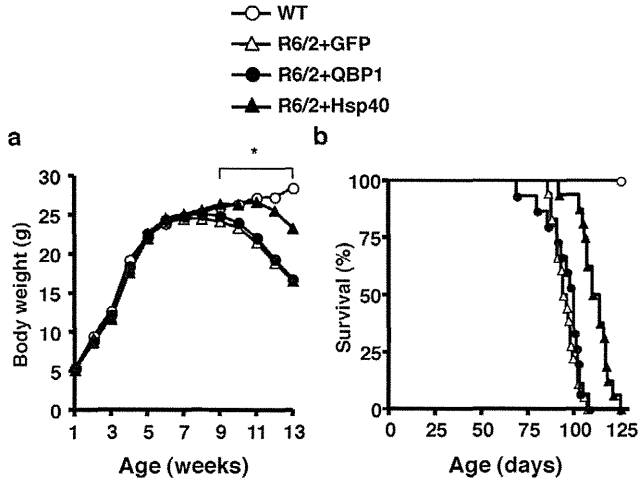

Figure 3. AAV5-Hsp40 improves body weight loss and extends the lifespan of polyQ disease mice. R6/2 mice at P7 were injected in both sides of the striatum with AAV5-GFP, AAV5-QBP1, or AAV5-Hsp40, and the following phenotypes were analyzed. (A) Body weight measured weekly. Values represent the mean (*$p<0.05$, R6/2+GFP vs R6/2+Hsp40). (B) Survival ($p<0.0001$, R6/2+GFP vs R6/2+Hsp40, Log-rank test). In both (A) and (B), n≥9 mice.
doi:10.1371/journal.pone.0051069.g003

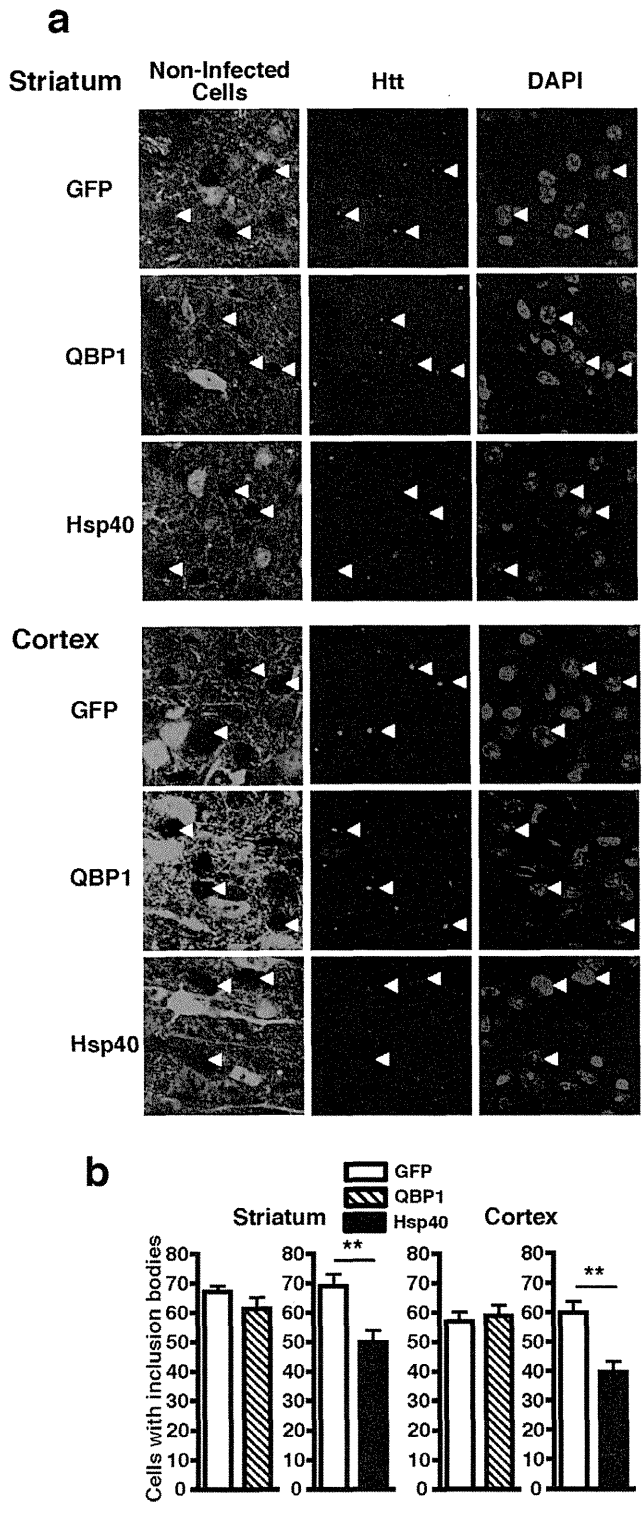

Figure 4. AAV5-Hsp40 also inhibits polyQ inclusion body formation in virus non-infected neurons of polyQ disease mouse brains. Htt inclusion body formation in 8 week old R6/2 mouse brains injected with AAV5-GFP on one side of the striatum and AAV5-QBP1 or AAV5-Hsp40 on the other side, was analyzed as in Fig. 1, but in the virus non-infected cells on each side of the brain. (A) Representative photographs of striatal (top panels) and cortical (bottom panels) sections of R6/2 mice injected with the indicated viruses. Green; virus infected cells, red; htt, and blue; nuclei visualized by DAPI staining. Representative virus non-infected cells in each panel are indicated by

white arrowheads. (B) Inclusion body formation in virus non-infected cells on the AAV5-QBP1 injected side and AAV5-Hsp40 injected side in the striatum (left) and cortex (right). Data are shown as means ± SEM of ≥6 fields of view, in which over 180 cells were counted (**$p<0.01$). Representative results of two mice analyzed are shown.
doi:10.1371/journal.pone.0051069.g004

$p<0.01$). The degree of inhibition was not as robust as in AAV5-Hsp40 infected neurons, but was still significant. These results raise a possibility that Hsp40 can exert a non-cell autonomous therapeutic effect on virus non-infected neurons in the brains of R6/2 mice, which is not observed with QBP1.

Hsp40 Inhibits Secretion of Pathogenic polyQ Proteins from Cultured Cells

We next aimed to elucidate the mechanism by which Hsp40 exerts its non-cell autonomous therapeutic effect in the brains of R6/2 mice. Recent studies suggest that prion-like cell-cell transmission of aggregation-prone proteins via their release from cells and subsequent uptake into neighboring cells, is involved in the spreading of neuropathology in the polyQ diseases as well as other neurodegenerative diseases [8–11]. We therefore hypothesized that Hsp40 may inhibit secretion of the pathogenic polyQ protein from cells to exert its non-cell autonomous therapeutic effect.

We used a cell culture model to test whether Hsp40 could inhibit secretion of a pathogenic polyQ protein from cells. An expanded polyQ stretch of 81 repeats fused with CFP and a V5 tag (Q81-CFP-V5) was co-expressed together with the GFP control, QBP1, or Hsp40 in Neuro2A cells. Twenty-four h later, the culture media were replaced with fresh media to remove all of the dead cells, and after a further 6 h of incubation, culture media were collected and concentrated using centrifugal filters, and subjected to Western blot analysis. Q81-CFP-V5 was detected in the culture medium of cells (Fig. 5A), suggesting that pathogenic polyQ proteins are secreted from cells. In cells co-expressing QBP1, the amount of Q81-CFP-V5 detected in the culture medium was similar to that in cells co-expressing GFP. In contrast, Neuro2A cells co-expressing Hsp40 showed ~40% less Q81-CFP-V5 in the culture medium compared with cells co-expressing GFP, suggesting that Hsp40 inhibits secretion of the pathogenic polyQ protein from cells (Figs. 5A,B). Furthermore, siRNA-mediated knockdown of endogenous Hsp40 increased the secretion of Q81-CFP-V5 by ~40% compared with cells treated with a control siRNA (Figs. 5C,D), indeed confirming that Hsp40 inhibits polyQ protein secretion. These results imply that inhibition of secretion of the polyQ protein from cells by Hsp40 results in a non cell-autonomous therapeutic effect in R6/2 mouse brains, possibly via inhibition of the cell-cell transmission of the pathogenic polyQ protein.

Discussion

In this study we show for the first time that viral vector-mediated expression of a molecular chaperone, namely Hsp40 significantly improves the neurological phenotypes of a mouse model of the polyQ diseases. Although a recent study reported the effectiveness of another Hsp40 family member, HSJ1a (DNAJB2a) in R6/2 mice, this study cannot be directly translated to a therapy since it was performed by the crossing of transgenic mice [30]. In addition, although lentiviral vector-mediated delivery of DNAJB2a to a polyQ disease rat model has been investigated [37], it did not demonstrate the therapeutic effect on the neurological phenotypes, perhaps because of the limited spread of lentiviruses. We successfully overcame these above problems by using AAV, which infects a widespread area of the brain, and is already used in human patients [38].

We did not detect significant therapeutic effects of AAV5-Hsp70 on R6/2 mice unlike AAV5-Hsp40, possibly due to the very low infection rate of our AAV5-Hsp70 (data not shown), or differences in the effectiveness of Hsp40 and Hsp70 against mutant htt. Indeed, previous studies examining the effect of Hsp70 in R6/2 mice have shown no or very modest therapeutic effects [28,29]. Furthermore, a cell culture study demonstrated that Hsp40 family members are effective against the toxicity of mutant htt, while Hsp70 family members are ineffective [35]. Taken together, these studies indicate that Hsp40 family members may be more effective than Hsp70 family members against the toxic effects of mutant htt.

We surprisingly found that AAV5-Hsp40 inhibits inclusion body formation also in virus non-infected cells (Fig. 4), suggesting a non cell-autonomous therapeutic effect. Aggregation prone proteins that cause neurodegenerative diseases including pathogenic polyQ proteins, as well as α-synuclein which causes Parkinson's disease, and tau which causes the tauopathies have recently been suggested to be transmitted between cells, and this may be the mechanism leading to the progressive spread of neuropathology in these diseases [8–11]. We detected a significant amount of the pathogenic polyQ protein in the culture medium of Neuro2A cells (Fig. 5A), suggesting its cell-cell transmission, which is compatible with previous studies [39,40]. We further found that Hsp40 suppresses secretion of the pathogenic polyQ protein from cells (Fig. 5), suggesting that it may inhibit the cell-cell transmission of the pathogenic polyQ protein. The non-cell autonomous therapeutic effect of Hsp40 may also involve other mechanisms, such as (1) AAV5-Hsp40 infected neurons may create a better environment for contacting non-infected neurons [41] or (2) Hsp40 itself may be secreted to exert therapeutic effects on neighboring non-infected neurons, as is suggested for Hsp70 [42].

We were unable to detect the therapeutic effect of AAV5-QBP1 on the neurological phenotypes of R6/2 mice, although we successfully detected its inhibition of inclusion body formation. However, we and others have previously shown that expression of QBP1 exerts therapeutic effects on the neurological phenotypes of *Drosophila* and mouse models of the polyQ diseases [16,17,43]. Since the infection efficiency of all of the viruses used in this study was quite low (~30%), the extent of neurons expressing QBP1 in the R6/2 mouse brains was probably insufficient to exert a detectable effect on the phenotypes. On the other hand, in the case of AAV5-Hsp40, inhibition of polyQ protein secretion which should lead to an increase in the number of rescued neurons, likely contributed to its improvement of the neurological phenotypes. Other possibilities may also contribute to their varying effects, for example (1) Hsp40 is more effective than QBP1 in inhibiting polyQ protein misfolding/aggregation, and (2) Hsp40 can also support the degradation of misfolded proteins [19], while QBP1 cannot.

In this study we demonstrate a therapeutic strategy against the polyQ diseases using AAV5-Hsp40, which has great potential for clinical application, since AAVs are safe and are widely utilized in clinical trials [38]. We further suggest a novel therapeutic mode of action of Hsp40, namely suppression of pathogenic polyQ protein secretion from cells, which may consequently suppress its cell-cell transmission. Since the transmission of aggregation-prone proteins is thought to be involved also in other neurodegenerative diseases, Hsp40 may exert a non-cell autonomous therapeutic effect on these other diseases. Elucidation of how Hsp40 inhibits polyQ protein secretion should reveal new therapeutic targets and

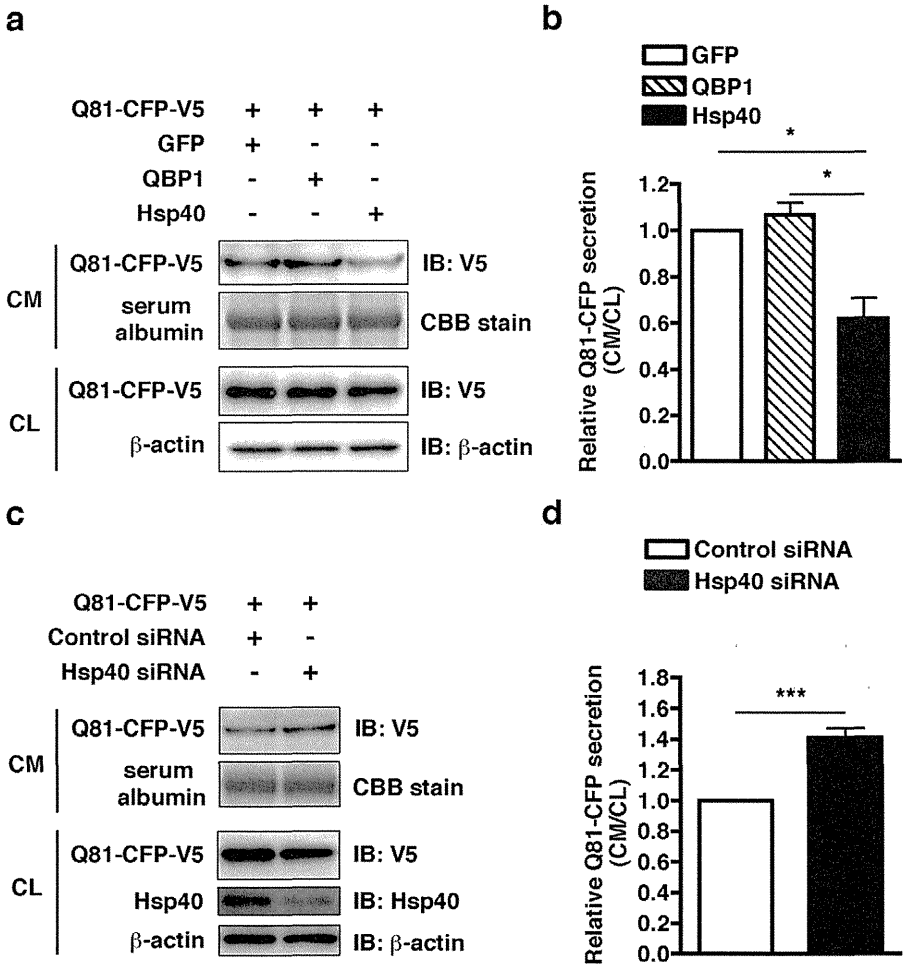

Figure 5. Hsp40 inhibits polyQ protein secretion in cultured cells. (A) Neuro2A cells were co-transfected with plasmids expressing Q81-CFP-V5 and either GFP, QBP1, or Hsp40, and the culture media (CM) and cell lysates (CL) were subjected to Western blot analysis with a V5 antibody to detect the Q81-CFP-V5 protein. (B) Relative amounts of Q81-CFP-V5 secreted into the culture media, calculated from the band intensities in (A), with the amount of Q81-CFP-V5 secreted from cells co-expressing GFP set to 1. (C) Neuro2A cells were transfected with a plasmid expressing Q81-CFP-V5 and siRNA against Hsp40 or a control siRNA, and the culture media (CM) and cell lysates (CL) were subjected to Western blot analysis with a V5 antibody to detect the Q81-CFP-V5 protein, and with an Hsp40 antibody. The loading controls are as in (A). (D) Relative amounts of Q81-CFP-V5 secreted into the cuture media, calculated from the band intensities in (C). In (A) and (C), serum albumin is shown as a loading control for the culture media, and β-actin as a loading control for the cell lysates. In (B) and (D), data are shown as means ± SEM of ≥ four independent experiments (*$p<0.05$, ***$p<0.001$).
doi:10.1371/journal.pone.0051069.g005

strategies for neurodegenerative diseases caused by aggregation-prone proteins.

Materials and Methods

Viral Vectors

Adeno-associated virus type 5 (AAV5) vector plasmids contained an expression cassette with a human cytomegalovirus enhancer/chicken β actin (CAG) promoter followed by the first intron of human growth hormone, target cDNA (either a tandem repeat of QBP1 fused to GFP [14], human Hsp40 (DNAJB1) [44], or GFP), and a simian virus 40 polyadenylation signal sequence, all positioned between the inverted terminal repeats of the AAV5 genome. AAV5 vectors were produced using the AAV5 plasmid, the AAV5 helper plasmid containing the rep and cap sequences from AAV5, as well as the pHelper plasmid from the AAV Helper-Free System containing the E2A, E4, and VA RNA genes of the adenovirus genome (Stratagene, La Jolla, CA). HEK293 cells were co-transfected with the AAV5 plasmid and two helper plasmids by the calcium phosphate method. Seventy-two h later, the cells were harvested and subjected to three rounds of freeze-thaw lysis. AAV5 vectors were then purified by two rounds of cesium chloride density gradient centrifugation. Vector titers were estimated by quantitative DNA dot-blot hybridization to be $\sim 0.2–1.6\times10^{13}$ genome copies/ml.

Animals

All animal experiments were performed in accordance with the guidelines of the Animal Ethics Committee of the National Institute of Neuroscience, National Center of Neurology and Psychiatry, Japan, and performed in accordance with the guidelines. Mice transgenic for human *huntingtin* exon 1 with approximately 150 CAG repeats (strain R6/2) [33] were obtained from the Jackson Laboratory (Bar Harbor, ME), and maintained on a B6CBAF1 background. Genotypes were analyzed and CAG repeat numbers of the transgenic mice were confirmed to be

similar by PCR as previously described [33]. Mice were housed on a 12-hour light/dark cycle, with food and water provided *ad libitum*. At least nine male R6/2 mice per group and wild-type littermate (WT) controls were used for the phenotype analyses, and two R6/2 mice were used for the inclusion body analyses.

AAV Injections

P7 old R6/2 mice were stereotaxically injected with 1 µl of virus solution (AAV5-GFP, AAV5-QBP1, or AAV5-Hsp40) into the striatum (coordinates 1 mm anterior to bregma, 2.25 mm lateral to the midline, and 3 mm ventral to the skull surface) at a rate of 0.1 µl/min using a 10 µl Hamilton syringe (Hamilton Company, Reno, NV) and an infusion pump (KD Scientific, Holliston, MA). For inclusion body analyses, AAV5-GFP was injected into one side of the striatum and AAV5-QBP1 or AAV5-Hsp40 into the other side. For phenotype analyses, the same virus was injected into both sides of the striatum.

Mouse Phenotype Analyses

For rotarod analysis, mice were tested at 4 and 7 weeks of age on an accelerating rotarod apparatus (Ugo Basile, Comerio, Italy) set to accelerate from 4 to 40 rpm over a period of 300 seconds. The time it took for each mouse to either fall off the rod or cling onto the rod for one full rotation was recorded. Mice were tested on the rod for three consecutive days, with three trials per day. The first day was regarded as training, and only the data from the second and third day were used. The highest and lowest values were excluded, and the middle four values were averaged. Grip strength analysis was performed at 9 and 12 weeks of age using a grip strength meter (Muromachi Kikai, Tokyo, Japan). Mice were placed gently by their tail on the metal grid of the meter so that they grip the grid with both forelimbs and hindlimbs, at which point they were pulled back gently with their tails, exerting a tension that is measured by the meter. Five trials were performed for each mouse, and the highest and lowest values were excluded and the middle three values were averaged. To measure open-field activity and rearing, mice at 5 and 8 weeks of age were tested using a spontaneous locomotor activity monitor (Supermex, Muromachi Kikai, Tokyo, Japan), consisting of an acrylic box of dimensions 40 cm×28 cm×31 cm with an activity sensor placed at the top and rearing sensors placed at the sides of the box. Mice were left in the box for a total of 15 min, and their activity count and rearing frequency were measured. For body weight analysis mice were weighed weekly. Mice were followed until their deaths in order to calculate their lifespans, a widely accepted and valuable parameter to assess therapeutic effects in these mice, which was approved by the institution's Animal Ethics Committee.

Tissue Preparation and Immunohistochemical Analyses

Mice were deeply anesthetized with sodium pentobarbital (100 mg/kg), and then perfused intercardially with saline followed by 4% paraformaldehyde (PFA) in phosphate-buffered saline (PBS). Brains were removed, post-fixed in 4% PFA in PBS at 4°C overnight, and then cryoprotected in 30% sucrose in PBS at 4°C for 24 h. Frozen 10 µm sections were cut using a cryostat. For immunohistochemical analysis, sections were blocked in PBS containing 5% goat serum and 0.1% Triton X-100 for 1 h at room temperature. The sections were then incubated with a mouse anti-huntingtin antibody (1:250; MAB5374, Millipore, Billerica, MA), and either a rabbit anti-Hsp40 antibody (1:500; SPA-400, Enzo Life Sciences, Farmingdale, NY) or a rabbit anti-GFP antibody (1:250; A11122, Invitrogen, Carlsbad, CA) at 4°C overnight, followed by an Alexa Fluor 596-conjugated goat anti-mouse IgG antibody and an Alexa Fluor 488 goat anti-rabbit IgG antibody (1:1000, Invitrogen) for 1 h at room temperature. Sections were mounted with Slowfade Gold antifade reagent with DAPI (Invitrogen) and examined using a confocal laser scanning microscope (FV1000; Olympus, Tokyo, Japan). The average fluorescence intensity of representative cells that were regarded as either "infected" or "non-infected" in each sample were measured using the Image J software, confirming that the two population of cells can readily be distinguished in the images (Fig. S3).

Cell Culture, Transfection and Western Blot Analysis

Neuro2A cells (obtained from ATCC) were grown and maintained in DMEM supplemented with 10% (v/v) FBS. Cells were plated on a 35-mm dish at a density of 4×10^5 cells per dish on the day before transfection. For the overexpression experiment, a plasmid vector encoding a tandem repeat of QBP1 fused to GFP, human Hsp40 [44], or GFP was transiently co-transfected with the Q81-CFP-V5 vector encoding an expanded polyQ stretch of 81 repeats fused with CFP and a V5 tag, using Lipofectamine LTX with PLUS reagent (Invitrogen). For the knockdown experiment, siRNA targeted against mouse Hsp40 (Santa Cruz Biotechnology, Santa Cruz, CA) or a control siRNA (RNAi Inc, Tokyo, Japan) was cotransfected with the Q81-CFP-V5 vector using Lipofectamine 2000 reagent (Invitrogen). At 24 h after transfection, culture media were replaced with fresh media, and after a further 6 h of incubation, culture media were collected and whole cell lysates were prepared with 1% Triton X in tris-buffered saline. For Western blot analysis, the culture media were concentrated using 30 kDa cutoff Amicon Ultra filters (Millipore). Q81-CFP-V5 in the concentrated culture media and whole cell lysates was separated using 10% SDS-PAGE gels and transferred onto PVDF membranes (Bio-Rad, Hercules, CA). The membranes were incubated overnight with an HRP-conjugated anti-V5 antibody (1:2500, Invitrogen) at 4°C. The HRP signal was visualized with SuperSignal West Femto Chemiluminescent Substrate (Thermo Fisher Scientific Inc, Rockford, IL), captured with a LAS-3000 mini CCD imaging system (Fujifilm, Tokyo, Japan), and band intensities were quantified using the Image J software. For the siRNA experiments, the membranes were then stripped and incubated with a rabbit anti-Hsp40 antibody (1:5000, SPA-400, Enzo Life Sciences Inc, Farmingdale, NY) at 4°C followed by an HRP-conjugated anti-rabbit IgG secondary antibody (1:10000, Thermo Fisher Scientific), and visualized as above.

Statistical Analyses

For the rotarod, open-field activity, rearing, grip strength and weight data, statistical analyses were performed by using one-way analysis of variance followed by Tukey's multiple comparison test to assess for significant differences between individual groups. The survival data was analyzed using the Log-rank test. For the inclusion body formation and Western blot analyses, Student's *t*-test was used. For all analyses, $p<0.05$ was considered as significant.

Supporting Information

Figure S1 AAV5 injection into the mouse striatum at P7 results in widespread expression of the transgene. R6/2 mice at P7 were injected in the right striatum with 1 µl of AAV5-QBP1, and 2 weeks later the expression of QBP1 was analyzed by immunohistochemistry. This widespread expression of QBP1 throughout the brain lasts for at least 13 weeks (data not shown). (PDF)

Figure S2 AAV5-QBP1 inhibits polyQ inclusion body formation in virus infected neurons of polyQ disease

mice. R6/2 mice at P7 were injected with AAV5-GFP on one side of the striatum and AAV5-QBP1 on the other side, and at 4, 8, and 14 weeks of age htt inclusion body formation in virus infected neurons of the striatum (left) and cortex (right) was assessed by immunohistochemistry. Data are shown as means ± SEM of ≥ 6 fields of view, in which over 180 cells were counted (*$p<0.05$, ***$p<0.001$). Representative results of two mice analyzed are shown.
(PDF)

Figure S3 AAV5 "infected" and "non-infected" cells can be clearly distinguished from their fluorescence intensity. The fluorescence intensity of representative cells that were regarded as either "infected" or "non-infected" in photographs of immunostained brain sections of R6/2 mice injected with either AAV5-GFP (left), AAV5-QBP1 (middle) or AAV5-Hsp40 (right). For each sample, a total of over 100 representative cells were analyzed from 5–6 fields of view.
(PDF)

Acknowledgments

We thank Kenzo Ohtsuka for the human Hsp40 cDNA, Yoshinaga Saeki and Hirokazu Hirai for helpful discussions, and Reiko Sasaki, Hirokazu Matsushima, Naomi Takino, Hitomi Miyauchi, and Keiko Ayabe for their technical assistance.

Author Contributions

Conceived and designed the experiments: HAP T. Takeuchi SM T. Toda KW YN. Performed the experiments: HAP T. Takeuchi HF KY CI HY. Analyzed the data: HAP T. Takeuchi T. Toda KW YN. Contributed reagents/materials/analysis tools: SM. Wrote the paper: HAP T. Takeuchi YN.

References

1. Gusella JF, MacDonald ME (2000) Molecular genetics: unmasking polyglutamine triggers in neurodegenerative disease. Nat Rev Neurosci 1: 109–115.
2. Orr HT, Zoghbi HY (2007) Trinucleotide repeat disorders. Annu Rev Neurosci 30: 575–621.
3. Michalik A, Van Broeckhoven C (2003) Pathogenesis of polyglutamine disorders: aggregation revisited. Hum Mol Genet 12 Spec No2: R173–186.
4. Shao J, Diamond MI (2007) Polyglutamine diseases: emerging concepts in pathogenesis and therapy. Hum Mol Genet 16 Spec No.2: R115–123.
5. Nagai Y, Popiel HA (2008) Conformational changes and aggregation of expanded polyglutamine proteins as therapeutic targets of the polyglutamine diseases: exposed β-sheet hypothesis. Curr Pharm Des 14: 3267–3279.
6. Williams AJ, Paulson HL (2008) Polyglutamine neurodegeneration: protein misfolding revisited. Trends Neurosci 31: 521–528.
7. Bauer PO, Nukina N (2009) The pathogenic mechanisms of polyglutamine diseases and current therapeutic strategies. J Neurochem 110: 1737–1765.
8. Aguzzi A, Rajendran L (2009) The transcellular spread of cytosolic amyloids, prions, and prionoids. Neuron 64: 783–790.
9. Brundin P, Melki R, Kopito R (2010) Prion-like transmission of protein aggregates in neurodegenerative diseases. Nat Rev Mol Cell Biol 11: 301–307.
10. Lee SJ, Desplats P, Sigurdson C, Tsigelny I, Masliah E (2010) Cell-to-cell transmission of non-prion protein aggregates. Nat Rev Neurol 6: 702–706.
11. Frost B, Diamond MI (2010) Prion-like mechanisms in neurodegenerative diseases. Nat Rev Neurosci 11: 155–159.
12. Bates G (2003) Huntingtin aggregation and toxicity in Huntington's disease. Lancet 361: 1642–1644.
13. Herbst M, Wanker EE (2006) Therapeutic approaches to polyglutamine diseases: combating protein misfolding and aggregation. Curr Pharm Des 12: 2543–2555.
14. Nagai Y, Tucker T, Ren H, Kenan DJ, Henderson BS, et al. (2000) Inhibition of polyglutamine protein aggregation and cell death by novel peptides identified by phage display screening. J Biol Chem 275: 10437–10442.
15. Nagai Y, Inui T, Popiel HA, Fujikake N, Hasegawa K, et al. (2007) A toxic monomeric conformer of the polyglutamine protein. Nat Struct Mol Biol 14: 332–340.
16. Popiel HA, Burke JR, Strittmatter WJ, Oishi S, Fujii N, et al. (2011) The aggregation inhibitor peptide QBP1 as a therapeutic molecule for the polyglutamine neurodegenerative diseases. J Amino Acids 2011: 265084.
17. Nagai Y, Fujikake N, Ohno K, Higashiyama H, Popiel HA, et al. (2003) Prevention of polyglutamine oligomerization and neurodegeneration by the peptide inhibitor QBP1 in *Drosophila*. Hum Mol Genet 12: 1253–1259.
18. Liberek K, Lewandowska A, Zietkiewicz S (2008) Chaperones in control of protein disaggregation. EMBO J 27: 328–335.
19. Kampinga HH, Craig EA (2010) The HSP70 chaperone machinery: J proteins as drivers of functional specificity. Nat Rev Mol Cell Biol 11: 579–592.
20. Hartl FU, Bracher A, Hayer-Hartl M (2011) Molecular chaperones in protein folding and proteostasis. Nature 475: 324–332.
21. Warrick JM, Chan HY, Gray-Board GL, Chai Y, Paulson HL, et al. (1999) Suppression of polyglutamine-mediated neurodegeneration in *Drosophila* by the molecular chaperone HSP70. Nat Genet 23: 425–428.
22. Kazemi-Esfarjani P, Benzer S (2000) Genetic suppression of polyglutamine toxicity in *Drosophila*. Science 287: 1837–1840.
23. Fernandez-Funez P, Nino-Rosales ML, de Gouyon B, She WC, Luchak JM, et al. (2000) Identification of genes that modify ataxin-1-induced neurodegeneration. Nature 408: 101–106.
24. Chan HY, Warrick JM, Gray-Board GL, Paulson HL, Bonini NM (2000) Mechanisms of chaperone suppression of polyglutamine disease: selectivity, synergy and modulation of protein solubility in *Drosophila*. Hum Mol Genet 9: 2811–2820.
25. Satyal SH, Schmidt E, Kitagawa K, Sondheimer N, Lindquist S, et al. (2000) Polyglutamine aggregates alter protein folding homeostasis in *Caenorhabditis elegans*. Proc Natl Acad Sci USA 97: 5750–5755.
26. Cummings CJ, Sun Y, Opal P, Antalffy B, Mestril R, et al. (2001) Over-expression of inducible HSP70 chaperone suppresses neuropathology and improves motor function in SCA1 mice. Hum Mol Genet 10: 1511–1518.
27. Adachi H, Katsuno M, Minamiyama M, Sang C, Pagoulatos G, et al. (2003) Heat shock protein 70 chaperone overexpression ameliorates phenotypes of the spinal and bulbar muscular atrophy transgenic mouse model by reducing nuclear-localized mutant androgen receptor protein. J Neurosci 23: 2203–2211.
28. Hansson O, Nylandsted J, Castilho RF, Leist M, Jaattela M, et al. (2003) Overexpression of heat shock protein 70 in R6/2 Huntington's disease mice has only modest effects on disease progression. Brain Res 970: 47–57.
29. Hay DG, Sathasivam K, Tobaben S, Stahl B, Marber M, et al. (2004) Progressive decrease in chaperone protein levels in a mouse model of Huntington's disease and induction of stress proteins as a therapeutic approach. Hum Mol Genet 13: 1389–1405.
30. Labbadia J, Novoselov SS, Bett JS, Weiss A, Paganetti P, et al. (2012) Suppression of protein aggregation by chaperone modification of high molecular weight complexes. Brain.
31. Okada T, Nomoto T, Shimazaki K, Lijun W, Lu Y, et al. (2002) Adeno-associated virus vectors for gene transfer to the brain. Methods 28: 237–247.
32. Davidson BL, Breakefield XO (2003) Viral vectors for gene delivery to the nervous system. Nat Rev Neurosci 4: 353–364.
33. Mangiarini L, Sathasivam K, Seller M, Cozens B, Harper A, et al. (1996) Exon 1 of the HD gene with an expanded CAG repeat is sufficient to cause a progressive neurological phenotype in transgenic mice. Cell 87: 493–506.
34. Bobo RH, Laske DW, Akbasak A, Morrison PF, Dedrick RL, et al. (1994) Convection-enhanced delivery of macromolecules in the brain. Proc Natl Acad Sci USA 91: 2076–2080.
35. Hageman J, Rujano MA, van Waarde MA, Kakkar V, Dirks RP, et al. (2010) A DNAJB chaperone subfamily with HDAC-dependent activities suppresses toxic protein aggregation. Mol Cell 37: 355–369.
36. Ross CA, Poirier MA (2005) Opinion: What is the role of protein aggregation in neurodegeneration? Nat Rev Mol Cell Biol 6: 891–898.
37. Howarth JL, Kelly S, Keasey MP, Glover CP, Lee YB, et al. (2007) Hsp40 molecules that target to the ubiquitin-proteasome system decrease inclusion formation in models of polyglutamine disease. Mol Ther 15: 1100–1105.
38. Muramatsu S, Fujimoto K, Kato S, Mizukami H, Asari S, et al. (2010) A phase I study of aromatic L-amino acid decarboxylase gene therapy for Parkinson's disease. Mol Ther 18: 1731–1735.
39. Ren PH, Lauckner JE, Kachirskaia I, Heuser JE, Melki R, et al. (2009) Cytoplasmic penetration and persistent infection of mammalian cells by polyglutamine aggregates. Nat Cell Biol 11: 219–225.
40. Herrera F, Tenreiro S, Miller-Fleming L, Outeiro TF (2011) Visualization of cell-to-cell transmission of mutant huntingtin oligomers. PLoS Curr 3: RRN1210.
41. Goodenough DA, Paul DL (2009) Gap junctions. Cold Spring Harb Perspect Biol 1: a002576.
42. Calderwood SK, Mambula SS, Gray PJ, Jr., Theriault JR (2007) Extracellular heat shock proteins in cell signaling. FEBS Lett 581: 3689–3694.
43. Bauer PO, Goswami A, Wong HK, Okuno M, Kurosawa M, et al. (2010) Harnessing chaperone-mediated autophagy for the selective degradation of mutant huntingtin protein. Nat Biotechnol 28: 256–263.
44. Ohtsuka K (1993) Cloning of a cDNA for heat-shock protein hsp40, a human homologue of bacterial DnaJ. Biochem Biophys Res Commun 197: 235–240.

Biochemical and Biophysical Research Communications 429 (2012) 18–23

Contents lists available at SciVerse ScienceDirect

Biochemical and Biophysical Research Communications

journal homepage: www.elsevier.com/locate/ybbrc

Calcium leak through ryanodine receptor is involved in neuronal death induced by mutant huntingtin

Mari Suzuki [a,b,*], Yoshitaka Nagai [b], Keiji Wada [b], Tatsuro Koike [a,c,*]

[a] Molecular Neurobiology Laboratory, Division of Life Science, Hokkaido University, Graduate School of Life Science, Sapporo 060-0810, Japan
[b] Department of Degenerative Neurological Diseases, National Institute of Neuroscience, National Center of Neurology and Psychiatry, 4-1-1 Ogawa-higashi, Kodaira, Tokyo 187-8502, Japan
[c] School of Life Science, Hosei University, Kajino, Koganei, Tokyo 184-8584, Japan

ARTICLE INFO

Article history:
Received 18 October 2012
Available online 3 November 2012

Keywords:
Polyglutamine
Ryanodine receptor
Calcium
Dantrolene
Neurodegeneration

ABSTRACT

Huntington's disease (HD) is a neurodegenerative disorder caused by an abnormal expansion of polyglutamine (polyQ) tract in huntingtin (htt) protein. Although altered calcium (Ca^{2+}) homeostasis is suggested in HD, its molecular mechanisms have remained poorly understood despite their important role in the pathogenesis. In this study, we examined involvement of ryanodine receptor (RyR), an endoplasmic reticulum-resident Ca^{2+} channel, in mutant htt-induced neuronal death. Inhibitors of RyR attenuated cell death induced by mutant htt, while co-expression of RyR enhanced htt toxicity. Intracellular Ca^{2+} imaging revealed that mutant htt caused excessive basal Ca^{2+} release (Ca^{2+} leak) through RyR leading to depletion of internal Ca^{2+} store. Ca^{2+} leak was also observed in striatal and cortical neurons from R6/2 HD model mice. Moreover, expression of FK506-binding protein 12 (FKBP12), a RyR stabilizer, suppressed both Ca^{2+} leak and cell death. These results provide novel evidence suggesting altered RyR function is involved in neuronal cell death, and its stabilization might be beneficial for treatment of HD.

1. Introduction

Huntington's disease (HD) is an autosomal dominant, fatal neurodegenerative disorder caused by an expansion of polymorphic CAG repeat encoding polyglutamine (polyQ) in huntingtin (htt) [1]. In this disease, progressive neuronal loss in the striatum and cerebral cortex resulted in abnormal involuntary movements and cognitive dysfunction [2]. Proteolytic N-terminal fragments of mutant htt containing the polyQ expansion are found to form inclusion bodies in affected neurons, and HD mice expressing exon1 of htt show neurological symptoms [3], suggesting that the truncated fragment of htt plays a crucial role in HD pathogenesis. It is generally thought that expanded polyQ stretch has been shown to confer toxic properties on the disease proteins through conformational transition to a β-sheet-dominant structure, leading to assembly of the host proteins into insoluble β-sheet-rich aggregates [4]. Toxic function of expanded polyQ has been assigned to various cellular regulatory systems including gene transcription, ubiquitin-proteasomal system, mitochondrial energy metabolism and calcium (Ca^{2+}) homeostasis [1]. However, molecular mechanisms centrally involved in mutant htt-induced neuronal death are not fully understood.

Altered Ca^{2+} homeostasis is one of the striking features of HD [5]. Our previous study demonstrated that perturbed intracellular Ca^{2+} homeostasis is associated with polyQ-induced neuronal death [6]. Endoplasmic reticulum Ca^{2+} stores are an important source of Ca^{2+} in neurons, and Ca^{2+} release through the inositol 1,4,5-triphosphate receptor (IP3R) or the ryanodine receptor (RyR) plays crucial role in neuronal survival and function [7]. Several groups have reported that altered function of IP3R is involved in polyQ toxicity [8–13]. It is noteworthy that a part of these studies showed therapeutic effect of dantrolene (Dan) on neurological phenotypes and cell loss in polyQ-disease model mice [8–11], although the target of Dan is not IP3R, but is RyR. Since Dan is a clinically approved RyR inhibitor, and its beneficial effects are widely demonstrated in various CNS disease models [14–16], it is expected to be clinically developed for HD and other related neurodegenerative diseases with no effective therapy currently available. However, the role of RyR, which is a target of Dan, in polyQ-induced neurodegeneration remains to be explored.

Abbreviations: HD, Huntington's disease; polyQ, polyglutamine; tNhtt, truncated N-terminal huntingtin; RyR, ryanodine receptor; IP3R, inositol 1,4,5-triphosphate receptors; Dan, dantrolene; RR, ruthenium red; Ry, ryanodine; DHBP, 1,1′-diheptyl-4, 4′-bipyridinium dibromide; 2APB, 2-aminoethoxydiphenyl borate; PEI, polyethyleneimine; TG, thapsigargin; $[Ca^{2+}]_i$, cytoplasmic Ca^{2+}; SERCA, sarco/endoplasmic reticulum Ca^{2+} pumps; FKBP12, FK506-binding protein..

* Corresponding authors: Address: Department of Degenerative Neurological Diseases, National Institute of Neuroscience, National Center of Neurology and Psychiatry, 4-1-1 Ogawa-higashi, Kodaira, Tokyo 187-8502, Japan. Fax: +81 42 346 1745 (M. Suzuki).

E-mail address: suzumari@ncnp.go.jp (M. Suzuki).

0006-291X/$ - see front matter © 2012 Elsevier Inc. All rights reserved.
http://dx.doi.org/10.1016/j.bbrc.2012.10.107

Here we demonstrated the involvement of RyRs in the mechanisms underlying mutant htt-induced neuronal death. We found that mutant htt causes Ca^{2+} leak from RyR in transiently transfected HD cellular model and neurons from R6/2 HD model mice. Moreover, expression of RyR stabilizing protein FK506-binding protein 12 (FKBP12) attenuated both Ca^{2+} leak and cell death. Our results provide novel evidence that altered RyR function may contribute to the neurodegeneration in HD.

2. Materials and methods

2.1. Materials

The sources of materials used in this work were as follows: 1,1′-diheptyl-4, 4′-bipyridinium dibromide (DHBP) from TOCRIS Cookson (Bristol, UK), 2-aminoethoxydiphenyl borate (2APB) from Calbiochem Corp. (La Jolla, CA), and thapsigargin from Research Biochemicals Inc. (Natiek, MA). All other materials were obtained either from Wako Pure Chemical Industries, Ltd. (Osaka, Japan) or from Sigma–Aldrich Corp (St. Louis, MO).

2.2. Plasmids

The truncated N-terminal huntingtin (tNhtt) tagged with green fluorescent protein (EGFP) expression constructs pEGFP-tNhtt17Q and pEGFP-tNhtt150Q were provided by N. Nukina [17]. Expression construct pBFP-tNhtt encoding blue fluorescent protein (BFP) was prepared by replacing the EGFP region of pEGFP-tNhtt with the BFP region from pQBI50fC1 vector. The expression plasmids of full-length RyR1 and FLAG-FKBP12 were from G. Meissner [18] and K. Miyazono [19], respectively.

2.3. Cell culture and transfection

Cortical or striatal neurons were prepared from neonatal Sprague–Dawley rats. All the experimental procedures conformed to the guidance set by the committee at the Research Center of Laboratory Animals, Hokkaido University. The tissues were digested with 0.05% trypsin followed by addition of feeding medium (Eagle's minimum essential medium [MEM] supplemented with 5% fetal calf serum [FCS], 5% heat-inactivated horse serum [HS], 10 mM HEPES pH 7.4, 20 mM glucose, 25 U/ml penicillin and 25 μg/ml streptomycin). Mechanically dissociated cells were plated on polyethyleneimine (PEI)-coated plastic plates or glass-cover slips and incubated at 36 °C in a humidified atmosphere of 5% CO_2/95% air. On day 2, Cytosine-β-D-arabinofuranoside (final 2.5 μM) was added to reduce the non-neuronal proliferation, and half of the medium was replaced with fresh serum-free medium at day 4. Cortical or striatal neurons were transfected at day 5–7 as described previously [20]. For co-transfection experiments an equimolar ratio mixture of the plasmids was used. Neuronal expression of tNhtts was confirmed by staining with anti-MAP2 (microtubule-associated protein 2, Sigma) antibody as described previously [6]. Human embryonic kidney 293t cells (293t cells) were cultured in Dulbecco's modified Eagle's medium supplemented with 5% FCS, penicillin and streptomycin.

2.4. Evaluation of cell death

Cortical or striatal neurons were incubated with 5 g/ml ethidium bromide (EtBr) in HEPES-buffered saline (HBS: 140 mM NaCl, 5 mM KCl, 1 mM $CaCl_2$, 1 mM $MgCl_2$, 20 mM HEPES, 1 g/L glucose, pH 7.2) for 5 min. Neurotoxicity is shown as a percentage of the number of neurons stained with EtBr out of that of EGFP-positive neurons. Cell viability of 293t cells was evaluated by dye extrusion with trypan blue as well. Experiments were repeated at least three times and representative results are presented.

2.5. Fluo-3 Ca^{2+} imaging

The cells were loaded with 3 μM fluo-3/AM (Dojindo Laboratories, Kumamoto, Japan) in HBS and 0.04% pluronic F147 (Molecular Probes Inc, Eugene, OR) for 30 min at 36 °C for 293t cells or 27–28 °C for mouse neurons. Ca^{2+} leak through RyR was assessed as described previously with slight modifications [21]. 2APB (final 100 μM) was added to the fluo-3 loading buffer. The glass-cover slips were mounted on a modified Sykes-Moore chamber (Bellco Biotechnology Inc., Vineland, NJ), placed on an inverted microscope (Nikon Diaphoto 300, Nikon). The data was analyzed using the software associated with ARGUS 50 (Hamamatsu Photonics Co., Hamamatsu, Japan). For striatal or cortical neurons from adult mice, HEPES-buffered Hank's balanced salt solution (H-HBSS) was used as a substitute for HBS.

2.6. Preparation of adult dissociated neurons

Striatal or cortical neurons were prepared from 13 to 14 weeks heterozygous transgenic R6/2 male mice (Jackson Laboratories, Bar Harbor, ME) or age-matched controls. Striatum and frontal cerebral cortex were removed from 350 μm coronal brain slices prepared by using McIlwain Tissue Chopper (Mickle Laboratory Engineering Co, Inc, Surrey, UK), and dissociated mechanically in Krebs–Ringer Bicarbonate buffer (KRBB) containing 0.1% bovine serum albumin. The cells were collected and incubated in a feeding medium (50% MEM, 25% H-HBSS, 25% heat-inactivated HS and 25 mM glucose) for 2 days, and then subjected to experiments.

2.7. Statistical analysis

Differences between two groups were analyzed by a two-tailed Student's *t* test. For comparison between more than two groups, ANOVA followed by *post hoc* Turkey's test was used.

3. Results

3.1. Inhibitors of ryanodine receptor protect neurons against toxicity of mutant huntingtin

In this study, we used cortical neurons transiently transfected with wild-type (17Q) or mutant (150Q) truncated N-terminal huntingtin (tNhtt) tagged with enhanced green fluorescent protein (EGFP). EGFP-tNhtt150Q formed intracellular inclusion body in the neurons (Fig. 1A), arrowheads, which is a typical hallmark of HD pathology, and caused neuronal cell death in a polyQ-length-dependent manner (Fig. 1B). By using this model, we explored the role of the inositol 1,4,5-triphosphate receptor (IP3R) and the ryanodine receptor (RyR) in mutant htt-induced neuronal death. We examined the effects of inhibitors of RyR or IP3R and found that dantrolene (Dan), ryanodine (Ry), 1,1′-diheptyl-4,4′-bipyridinium dibromide (DHBP) and ruthenium red (RR), all inhibitors of RyRs, significantly suppress mutant htt-induced neuronal death (Fig. 1C). In contrast, 2-aminoethoxydiphenyl borate (2APB), an inhibitor of IP3Rs, failed to protect these neurons. The protective effect of Dan was abolished by 4-chloro-m-cresol (CMC), a potent activator of RyRs, confirming that the effect of Dan is indeed mediated by inhibition of RyR (Fig. 1D). It was also found that Dan effectively attenuated mutant htt-induced cell death of striatal neurons (Fig. 1E). These results indicate that inhibition of Ca^{2+} release from RyRs, but not IP3Rs, attenuates neuronal death induced by mutant htt.

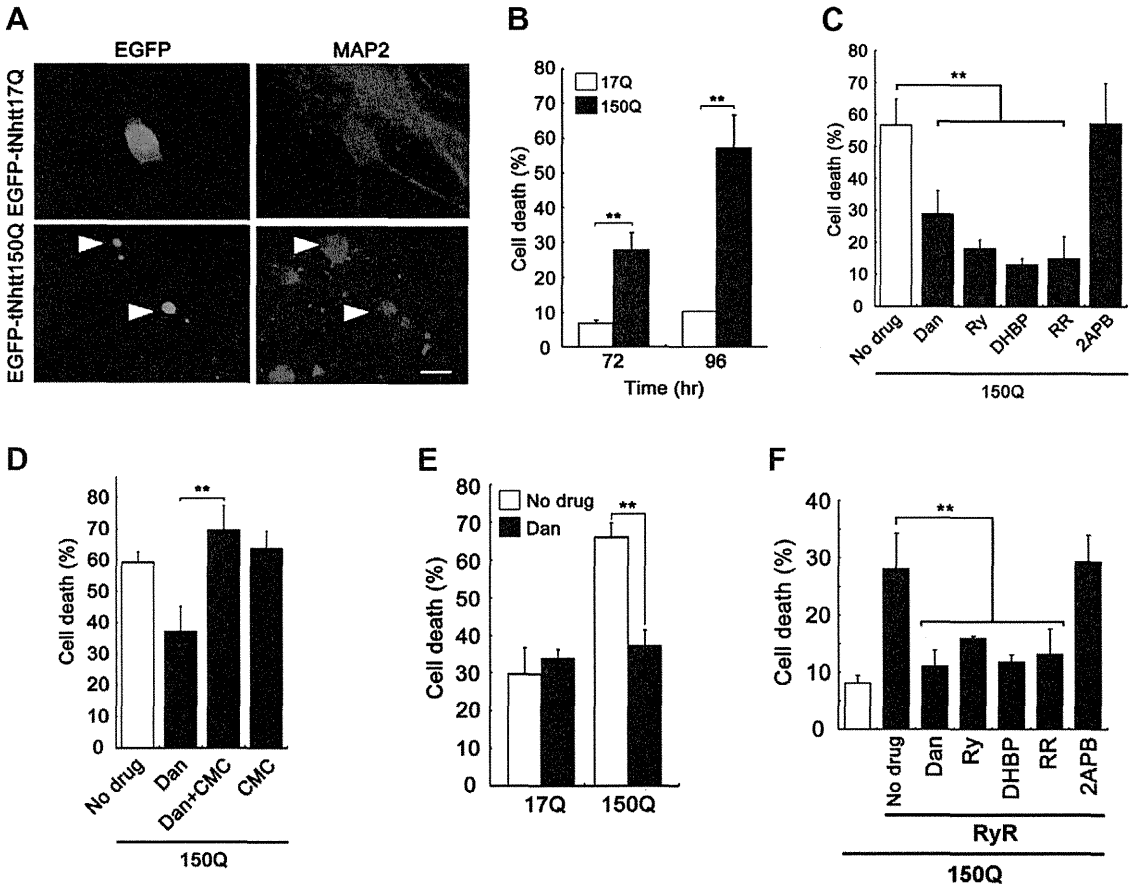

Fig. 1. Blockade of ryanodine receptor (RyR) attenuates neuronal cell death induced by mutant huntingtin (htt). (A) Immunofluorescence analysis. Cortical neurons transfected with EGFP-tagged truncated N-terminal huntingtin 17Q (EGFP-tNhtt17Q) and 150Q (EGFP-tNhtt150Q) were stained with the neuronal marker MAP2. Arrowheads indicate mutant htt inclusions. Bar, 10 μm. (B) Time- and length-dependency of mutant htt-induced neuronal death. (C) Suppression of mutant htt-induced neuronal death by inhibition of RyRs. Cortical neurons transfected with EGFP-tNhtt150Q (150Q) were treated with RyR inhibitors such as dantrolene (Dan, 30 μM), ryanodine (Ry, 10 μM), 1,1′-diheptyl-4,4′-bipyridinium dibromide (DHBP, 50 nM) or ruthenium red (RR, 10 nM). Inositol 1,4,5-triphosphate receptors (IP3Rs) inhibitor 2-aminoethoxydiphenyl borate (2APB, 10 μM) did not show any effects. (D) Counteracting effect of RyR activator 4-chloro-m-cresol (CMC) on the protective effect of Dan. Cortical neurons were treated with Dan (30 μM), CMC (10 μM), or both. (E) Protective effect of Dan in striatal neurons. Concentration of Dan was 30 μM. (F) Potentiation of mutant htt toxicity by expression of RyR1. HEK 293t cells bearing no endogenous RyR, were co-transfected with EGFP-tNhtt150Q (150Q) and RyR1. Concentration of the drugs was same as C. The mean ± SD ($n = 3$). $^{**}p < 0.01$.

To obtain direct evidence that RyRs actually mediate the toxicity of mutant htt, we next investigated the effect of RyR expression on mutant htt toxicity. Co-expression of EGFP-tNhtt150Q and RyR1, which has target site for Dan inhibition [22], and is reported to increase in the caudate nucleus of HD patients [23], significantly increased cell death of HEK 293t (293t) cells bearing no endogenous RyRs. We further confirmed that this increase was suppressed by RyRs inhibitors, but not with IP3Rs inhibitor (Fig. 1F). Taken together, we concluded that abnormal Ca^{2+} release through RyR1 is induced by mutant htt and involved in mutant htt-induced neuronal cell death.

3.2. Mutant htt causes abnormal Ca^{2+} leak through RyRs

We moved on to measure the level of cytoplasmic calcium ($[Ca^{2+}]_i$) upon activation of RyRs to examine if there is any dysfunction regarding Ca^{2+} release from RyR expressing mutant htt. The cells co-expressing blue fluorescent protein (BFP)-tNhtts and RyR1 responded to caffeine, which activates RyRs to release Ca^{2+} from ER to cytoplasm, by rapid increases in $[Ca^{2+}]_i$ 24 h after transfection, and the responses were similar between wild-type (Q17) and mutant (Q150) htt (Fig. 2A and B). However, the cells expressing mutant htt became to poorly respond to this stimulation at 48 h, and these cells failed to respond by 72 h.

These results raise the possibility that the internal Ca^{2+} store might be depleted under these conditions by enhanced spontaneous Ca^{2+} release (Ca^{2+} leak). Ca^{2+} levels of cytoplasm and ER is balanced by uptake through SERCAs (sarco/endoplasmic reticulum Ca^{2+} pumps) and release through RyRs and IP3Rs (Fig. 3A). Therefore, Ca^{2+} leak through RyR could be evaluated by measuring $[Ca^{2+}]_i$ increase under treatment with thapsigargin (TG), an inhibitor of SERCAs, following pretreatment with 2APB, an inhibitor of IP3Rs [21]. Upon these treatments, there was a slight increase in $[Ca^{2+}]_i$ in the cells expressing wild-type htt and RyR1 (17Q), which indicates spontaneous Ca^{2+} release through RyR1. Compared with this, there was a large increase in $[Ca^{2+}]_i$ in the cells expressing mutant htt and RyR1 (150Q, Fig. 3B and C). This $[Ca^{2+}]_i$ increase was suppressed by treatment with RyR inhibitor DHBP (150Q+DHBP), suggesting that excessive Ca^{2+} leak through RyR is induced by mutant htt.

Next we further sought to obtain evidence that abnormal Ca^{2+} leak from RyRs occurs in a well-established animal model as well. Striatal or cortical neurons were prepared from 13- to 14-weeks-old R6/2 HD model mice expressing exon1 of htt with 144 repeats of polyQ tract, and subjected to Ca^{2+} imaging. The neurons from R6/2 (R6/2) mice, but not those from age-matched wild-type mice (WT), showed a gradual increase in $[Ca^{2+}]_i$ levels following application of TG (Fig. 3D) and there was a significant difference in relative

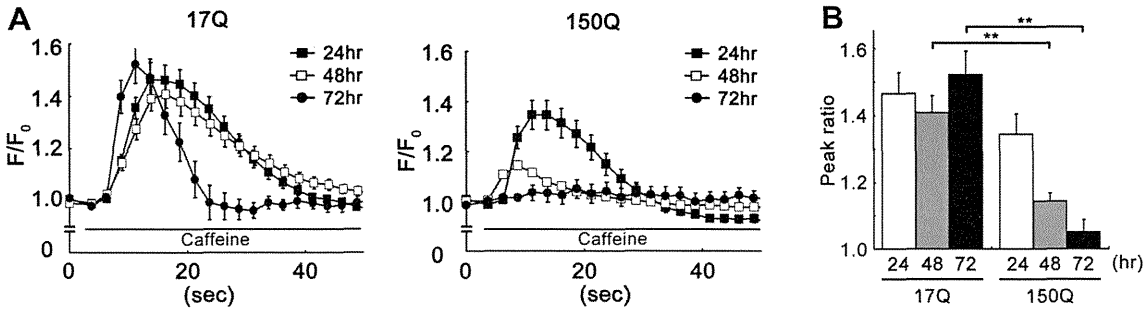

Fig. 2. Caffeine-sensitive Ca^{2+} store declines in the cells expressing mutant htt. (A) Cytoplasmic Ca^{2+} increase upon treatment with an activator of the RyR. HEK 293t cells were co-transfected with RyR1 and blue fluorescent protein (BFP)-tagged tNhtt17Q (17Q) or 150Q (150Q) for 24, 48 or 72 h, and then loaded with calcium indicator fluo-3. Fluo-3 fluorescence of BFP-positive cells was monitored following treatment with caffeine (25 mM). (B) Peak values of caffeine responses in A. A maximal value for F/F_0 was calculated for caffeine responses of each cell. The mean ± SE (n = 16–26 cells). $^{**}p < 0.01$.

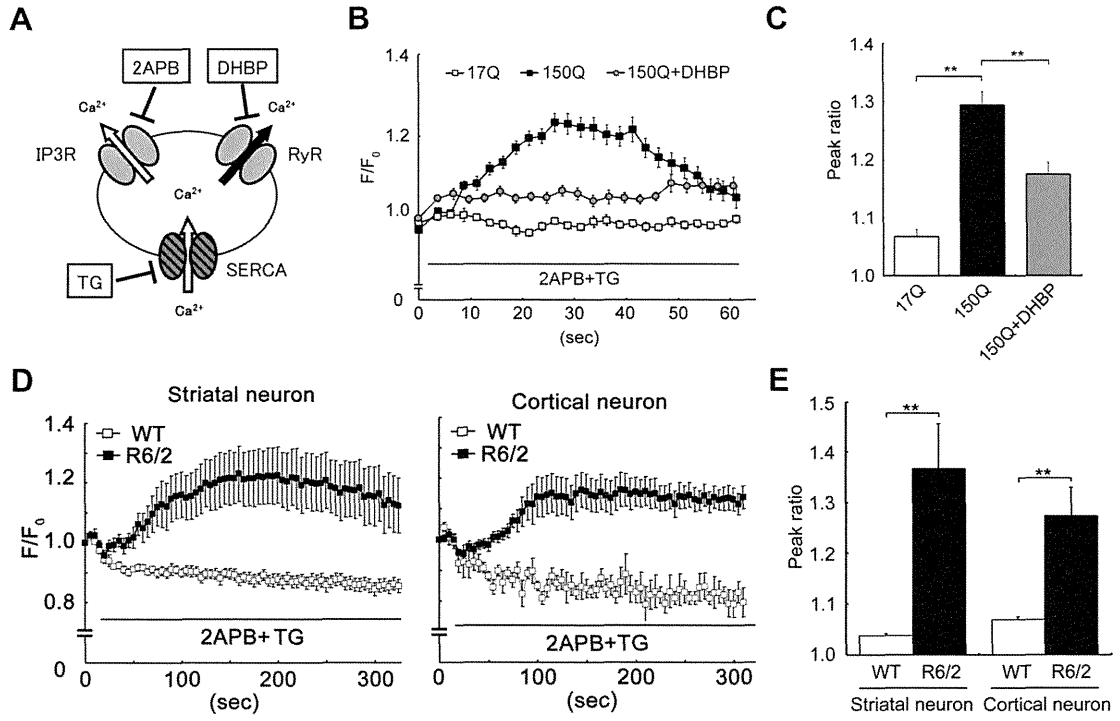

Fig. 3. Mutant htt induces abnormal Ca^{2+} leak through RyRs. (A) Schematic drawing of Ca^{2+} flow between cytoplasm and ER. Ca^{2+} leak through RyR was assessed by measurement of cytoplasmic Ca^{2+} increase upon treatment with thapsigargin (TG), an inhibitor of SERCAs (ER Ca^{2+} pumps), and 2APB, an inhibitor of IP3Rs. (B) Abnormal Ca^{2+} leak through RyR in the cells expressing mutant htt. HEK 293t cells were transfected with RyR1 and BFP-tNhtt17Q (17Q) or 150Q (150Q). At 24 h of transfection, the cells were loaded with fluo-3 in the presence of 100 μM 2APB and then cytoplasmic Ca^{2+} levels were measured following treatment with 1 μM TG. Enhanced Ca^{2+} increase of mutant htt-expressing cells was suppressed by RyR inhibitor DHBP (50 nM). The mean ± SE (n = 13–29). (C) Maximal value of F/F_0 in B. (D) Abnormal Ca^{2+} leak in striatal or cortical neurons from R6/2 HD model mice. The neurons prepared from 13- to 14-week-old wild-type (WT, n = 15) or R6/2 mice (R6/2, n = 14) were incubated with 3 μM fluo-3 and 100 μM 2APB. Then, cytoplasmic Ca^{2+} levels were measured following treatment with 0.5 μM TG. (E) Quantification of the results in D. The mean ± SE. $^{**}p < 0.01$.

peak ratios of these responses between R6/2 and wild-type mice (Fig. 3E). Taken together, these results show that mutant htt induces enhanced Ca^{2+} leak through RyRs in the HD pathogenesis.

3.3. Expression of RyR stabilizer FKBP12 suppresses mutant htt-induced abnormal Ca^{2+} leak and cell death

We further examined whether stabilization of RyR1 could suppress abnormal Ca^{2+} leak and mutant htt-induced cell death. It is well-known that FK506-binding protein 12 (FKBP12), a member of immunophilin family, physically interacts and stabilizes RyR1 by decreasing channel open probability, playing the role for endogenous RyR stabilizer [24]. Therefore, we co-expressed FKBP12 with mutant htt, and found that mutant htt-induced Ca^{2+} leak through RyR1 was effectively suppressed by FKBP12 in 293t cells (Fig. 4A and B). Consistent with these results, FKBP12 decreased cell death of 293t cells, primary cultured cortical and striatal neurons (Fig. 4C and D), suggesting that stabilization of RyR channel function protects neurons against mutant htt toxicity.

4. Discussion

Here we have shown that inhibitors of RyRs attenuate cell death induced by mutant htt. Mutant htt caused Ca^{2+} leak from RyR1 followed by depletion of Ca^{2+} store in the ER, and expression of RyR stabilizer FKBP12 suppressed both Ca^{2+} leak and cell death. From these results we concluded that abnormal Ca^{2+} leak from RyRs may contribute to neuronal death in HD.